Asian Journal of Chemistry; Vol. 33, No. 10 (2021), 2313-2320

ASIAN JOURNAL OF CHEMISTRY

https://doi.org/10.14233/ajchem.2021.23308

Investigating Potential Part of α-Santonin in the Treatment of SARS-CoV-2 and Cervical Cancer based on Molecular Docking Strategy

S. JEYAVIJAYAN[1,*], M. RAMUTHAI[1] and PALANI MURUGAN[2]

[1]Department of Physics, Kalasalingam Academy of Research and Education, Krishnankoil-626126, India
[2]Department of Physics, Dr. B.R. Ambedkar Institute of Technology, Port Blair-744103, Andaman & Nicobar Islands, India

*Corresponding author: E-mail: sjeyavijayan@gmail.com

Received: 15 May 2021; *Accepted*: 8 July 2021; *Published online*: 20 September 2021; AJC-20500

The widespread of severe acute respiratory syndrome coronavirus 2 (SARS-CoV-2) has been posturing extraordinary dangers globally. Additionally, cervical cancer is also the most predominant threatening tumor among ladies around the world. The investigation has progressively centered on improving treatments, such as anti-angiogenic and anti-hepatoma drugs. The conceivable inhibitory action of α-santonin, which has a good interacting affinity with the active protein sites of human SARS-COV-2 and cervical cancer was screened in this work. The molecular properties such as NBO, MEP, HOMO-LUMO, Mulliken charge and NMR studies have been performed by the DFT-B3LYP strategy. Present computational outcomes explain that α-santonin particle can be utilized as a specialist within the worldwide fight against SARS-CoV-2 and cancer treatment.

Keywords: SARS-CoV-2, Docking studies, α-Santonin, Cervical cancer.

INTRODUCTION

Human coronaviruses (HCoVs) are responsible for several serious respiratory maladies such as common cold, pneumonia and bronchiolitis. HCoVs have been affecting in different places around the world and connected with major outbreaks of deadly human pneumonia. The first CoV explosion as serious intense respiratory disorder coronavirus (SARS-CoV) started in November 2002 at Foshan, China. Afterward that was turned into worldwide contamination in 2003 with a deadly rate of 10% around the world. Taking after one decade, the moment HCoV widespread was caused by center east respiratory disorder coronavirus in June 2012 at Jeddah, Saudi Arabia, with a worldwide casualty rate of 35%. Later the third major HCoV blast, which happened in December 2019 in Wuhan territory of China, caused by an exceedingly homologous strain as a serious intense respiratory disorder coronavirus 2 (SARS-CoV-2); now designated the disease as Coronavirus illness 2019 (COVID-19). These HCoVs episodes are classified as a non-stop risk to people and the world economy since of their unpredicted development, fast and simple multiplication that driven to harmful results [1].

On the other hand, cancer is another leading causes of mortality in the world with a predominance of > 10 million death per year [2]. Current cancer medications incorporate surgical intercession, radiation and taking chemotherapeutic drugs, which frequently murder the sound cells and result in toxicity in patients. In this manner, analysts are seeking out ways to be able to dispose of fair cancerous cells. In current scenario, cervical cancer is the 4th most common cancer among ladies and proceeds to be a major health concern [3,4]. Concurrent chemoradiation (CCRT) is the standard treatment for locally progressed cervical cancer (LACC) with survival rates of 30-80% [5,6]. A few endeavors have been made to move forward the result of caring in terms of infection control and dealing-related toxicities.

The α-santonin contains many isoprenes and shows numerous biological activities such as antipyretic, anti-inflammatory, anthelmintic and antifungal [7]. The functionalized ring with lactone and dienone systems leads the molecule in important anticancer activities [8]. Also, α-santonin allows many centres for reactivity that offer chance for more chemical alterations to generate novel drug systems [9]. As of now, the spectroscopic examination and DFT calculations of α-santonin were

reported by Palani *et al*. [10] but no molecular docking investigation and further studies have been carried out. Thus, an endeavor has been made to investigate the role of α-santonin for improving the treatment of SARS-CoV-2 and cervical cancer by molecular docking. The other molecular properties of α-santonin have been performed by the DFT-B3LYP strategy, which can support pharmaceuticals and natural drugs.

COMPUTATIONAL METHODS

SARS-CoV-2 surface proteins: The main protein markers for SARS-CoV-2 are extracted from the site (https://www.rcsb.org/) and www.pdb.org.(pdb - protein data bank) [11]. The target structures of SARS-CoV-2 such as 7DDN, 7DDD, 7AD1 and 7DK3 is processed for molecular docking examination [12,13]. For cervical cancer, the human papillomavirus class 59 (5JB1) protein was considered for docking interaction. Target adaptability is the most troubles in protein-ligand process. We tended to this issue by putting away a few passages for the equivalent protein co-crystallized with the distinctive ligands. Discovery Studio (Version: 2017 R2 client) was utilized to assess the assembly of protein and amino corrosive position, trailed by docking with α-santonin.

Molecular docking: Auto Dock Vina (version: 4.2.1) was operated to perform the docking strategy [14]. MGL Apparatuses 1.5.4 was utilized to develop the ligand and receptor. To calculate the protonation of input assemblies, hydrogen atoms are connected to the ligand and receptor. The configuration file is created using the box size and receptor coordinates. For each screened ligand, we added hydrogen as well as conceivable molecular torsions [14]. To measure the docking energy affinities (Kcal/Mol), protein and ligand structures are also saved in pdbqt setup. For each ligand, Auto Dock Vina delivered energy values for ten distinctive docking postures.

Auto dock vina's results are evaluated for each calculation to get the binding energies of each complex, considering the root mean square deviation (RMSD) between the introductory and consequent structures, owing to the compliance of the ligand within the dynamic location of qualities. To anticipate the molecular properties of bioactive compounds, Discovery Studio 2017 R2 Client program was utilized to degree molecular weight, H-bond acceptor destinations, bond number and Lipinski's law [15]. The Studio 2017 R2 Client [16] was utilized to tally the number of H bonds and non-covalent intelligence in each complex and create statistics of the complexes and interaction plots. The other possessions of α-santonin such as NBO, MEP, HOMO-LUMO, Mulliken charge and NMR examination have been accomplished by the DFT-B3LYP [17,18] method using Gaussian 09W software package [19].

RESULTS AND DISCUSSION

Molecular docking analysis: Molecular docking has ended up a progressively imperative apparatus for medicate disclosure. This approach can be utilized to show the interaction between a small molecule and a protein, which permits to characterize the behaviour of molecules within the official location of target proteins as well as to explain the principal biochemical forms [20]. The optimized structure of α-santonin is shown in Fig. 1. In this work, α-santonin molecule was applied as a ligand and SARS-CoV-2 related proteins such as S protein at open state, Spike, S trimer (S-open) and S protein at closed state [PDB ID: (a) 7DDN, (b) 7AD1, (c) 7DK3, (d) 7DDD], were used as targeted proteins. The α-santonin has been docked with the four chosen focused on proteins, which gives the least binding energy, inhibition consistent values and intermolecular energy of the composites are delineated in Fig. 2 and binding data are given in Table-1. The outcomes indicate that the α-santonin has the lower binding and inhibition constant values for the target SARS-Cov2 S protein at open state (7DDN). These results will be valuable in the *in vitro* and *in vivo* works for the development of drugs in the treatment of SARS-CoV-2 disease. Hence, it is sensible to speculate that α-santonin might have powerful SARS-CoV-2 action and the comparison plot for different proteins is as appeared in Fig. 3.

Also, the *in silico* molecular docking investigation reveals that the α-santonin interacts with the cervical cancer marker protein which incorporates human papillomavirus (HPVs). HPVs are accepted to be the major connective pathogens of

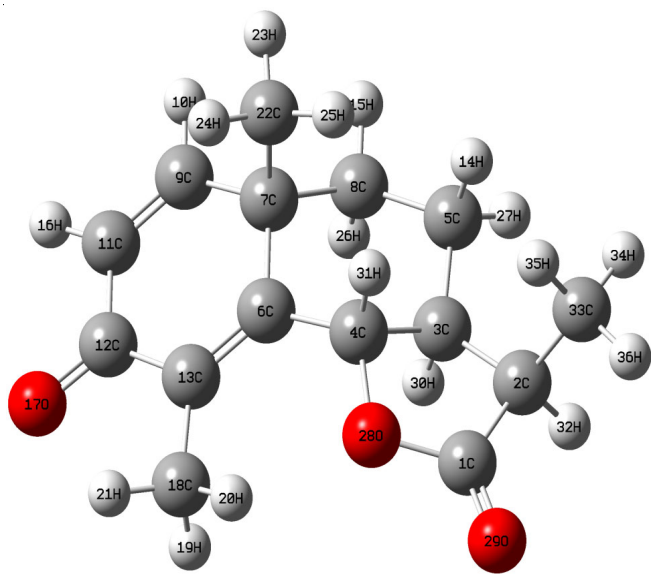

Fig. 1. Molecular structure of α-santonin

TABLE-1
CALCULATION DEPICTING INTERACTING BINDING SITE RESIDUES AND ATOMS ELABORATED IN H-BONDING

Protein name	Binding energy	Ligand efficiency	Inhibit constant	Intermol energy	Ligand and protein atom involved in H-bonding
SARS-Cov2 S protein at open state	-9.3	-0.70	33.560	-9.37	THR A, THR C, THR B
SARS CoV2 Spike	-8.5	-0.50	234.60	-8.45	SER, VAL, THR C
SARS-CoV-2 S trimer, S-open	-8.2	-0.69	280.99	-8.78	PHE B, ARG, PHE C, LEU
SARS-Cov2 S protein at closed state	-9.2	-1.00	41.090	-9.43	LYS, THR B, GLU, ASN, ALA

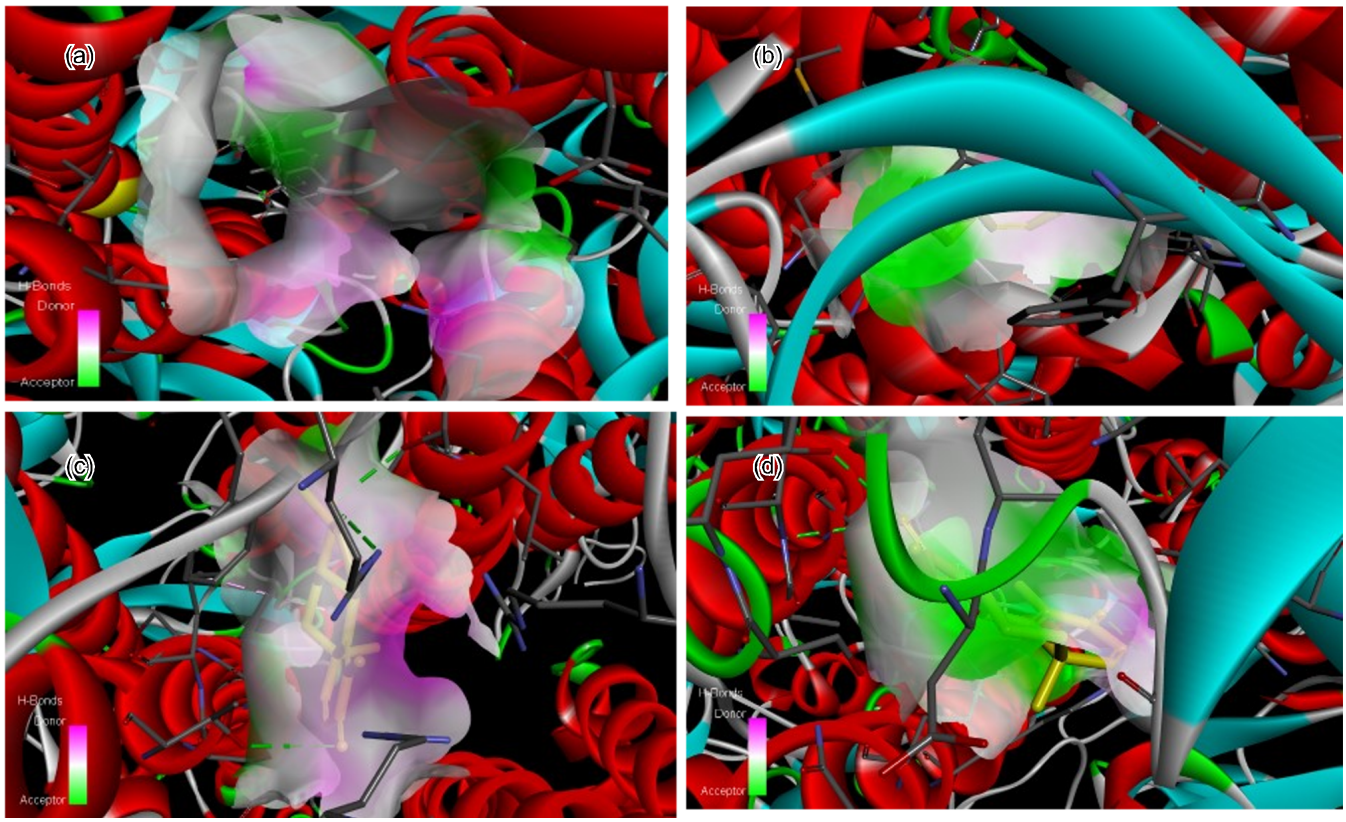

Fig. 2. Ligand-receptor interactions for (a) 7DDN, (b) 7AD1, (c) 7DK3, (d) 7DDD] with α-santonin

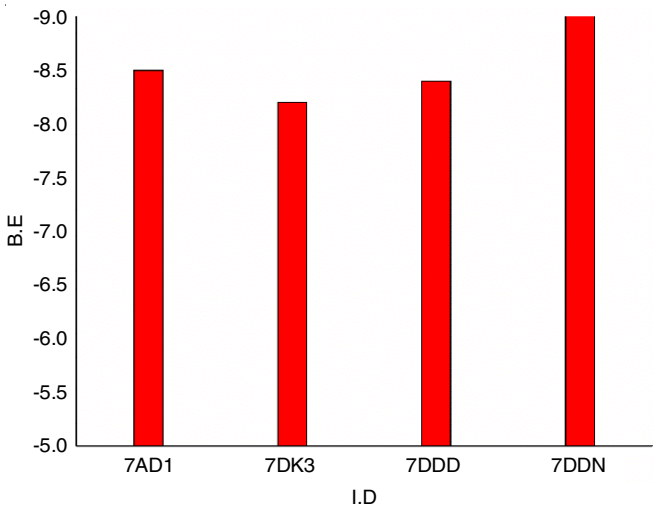

Fig. 3. Plot of varies proteins with targeted ligand interactions

cervical cancer. Fig. 4 gives the 3D representation of docked ligand (α-santonin) at the binding location of the hydrogen bonds ARG, TYR, LEU, GLN, LYS with a focus on protein ID: 5JB1. The binding free energy (ΔGº) for 5JB1 was found to be -9.20 KJ mol^{-1}.

Molecular electrostatic potential surface analysis: Molecular electrostatic potential (MEP) surface is utilized to get the responsive sites and hydrogen interactions [21]. This surface makes a difference to find the reactive points of the molecule by considering its colour codes. In MEP surface investigation, the foremost negative, positive, neutral electrostatic

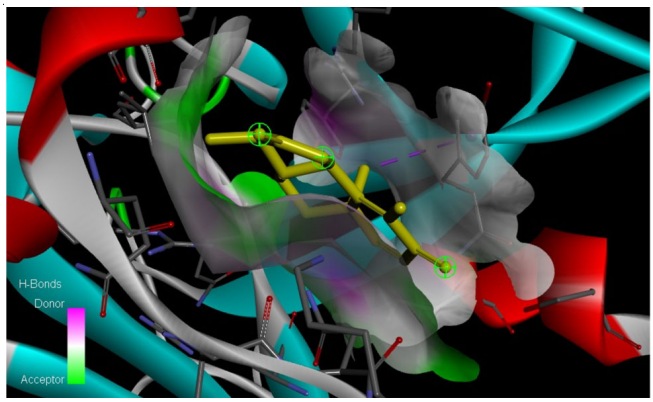

Fig. 4. 3D ligand interactions with 5JB1 protein

potential is representing to the reddish, blue, green codes, respectively. The MEP surface of α-santonin is portrayed in Fig. 5. The electrophilic region of the α-santonin is covering the O17 and O29. The other electronegative atom O28 is partially negative character because it is prepared to be bonding with another adjacent molecular system. The blue regions are enveloping all H atoms of α-santonin but primarily in H31.

Natural bond orbital (NBO) analysis: NBO examination gives a productive strategy for considering intra and intermolecular bonding and gives a helpful premise for examining the charge exchange or conjugative interaction in molecular frameworks [22]. Consequently, the analysis of α-santonin molecule is performed at the DFT/B3LYP strategy and the calculated values are given in Table-2. The higher energy of E(2) in NBO

TABLE-2
NATURAL BOND ORBITAL (NBO) ANALYSES FOR α-SANTONIN

Donor (i)	ED (i) (e)	Acceptor (j)	ED (j) (e)	Stabilization energy, E(2) (kJ mol^{-1})	Energy difference between donor and acceptor E(j)–E(i) (a.u.)	Fock matrix element, F (i,j) (a.u.)
σ (C1-O29)	0.99804	σ*(C9-C11)	0.00707	92.32	0.30	0.209
π (C1-O29)	0.99643	σ*(C13-C18)	0.00823	35.02	0.13	0.086
σ (C3-H30)	0.98608	σ*(C5-C8)	0.00605	117.92	1.21	0.478
		σ*(C9-C11)	0.00707	1686.38	0.37	0.995
		σ*(C11-H16)	0.00715	243.25	1.04	0.638
		π*(C12-O17)	0.11130	89.77	0.96	0.390
		σ*(C13-C18)	0.00823	312.57	0.91	0.677
		σ*(C18-H21)	0.00432	153.26	1.21	0.545
		σ*(C33-H35)	0.00338	59.15	1.41	0.366
σ (C5-H27)	0.98910	σ*(C11-H16)	0.00715	32.35	0.41	0.145
		σ*(C13-C18)	0.00823	53.29	0.28	0.153
σ (C6-C7)	0.97935	σ*(C5-C8)	0.00605	94.93	1.18	0.425
		σ*(C9-C11)	0.00707	1455.58	0.34	0.893
		σ*(C11-H16)	0.00715	200.73	1.02	0.574
		π*(C12-O17)	0.11130	74.99	0.93	0.350
		σ*(C13-C18)	0.00823	311.43	0.89	0.668
		σ*(C18-H21)	0.00432	125.77	1.18	0.490
		σ*(C33-H35)	0.00338	47.38	1.38	0.326
π(C6-C13)	0.92575	π*(C12-O17)	0.11130	103.40	0.05	0.092
σ(C7-C8)	0.97854	σ*(C3-C4)	0.01696	30.03	1.40	0.259
		σ*(C4-C6)	0.01556	30.21	1.46	0.266
		σ*(C5-C8)	0.00605	109.64	1.22	0.464
		σ*(C9-C11)	0.00707	1579.14	0.38	0.979
		σ*(C11-H16)	0.00715	217.95	1.05	0.610
		π*(C12-O17)	0.11130	80.78	0.97	0.371
		σ*(C13-C18)	0.00823	280.81	0.92	0.647
		σ*(C18-H21)	0.00432	136.72	1.22	0.464
		σ*(C33-H35)	0.00338	51.85	1.42	0.346
σ(C8-H15)	0.99107	σ*(C11-H16)	0.00715	42.45	0.42	0.169
		σ*(C13-C18)	0.00823	69.48	0.29	0.179
σ(C9-C11)	0.99145	σ* (C3-C4)	0.01696	36.33	2.06	0.348
		σ*(C4-C6)	0.01556	37.26	2.13	0.357
		σ*(C5-C8)	0.00605	120.52	1.88	0.602
		(σ*C9-C11)	0.00707	976.79	1.04	1.274
		σ*(C11-H16)	0.00715	269.07	1.72	0.859
		π*(C12-O17)	0.11130	85.55	1.64	0.499
		σ*(C13-C18)	0.00823	301.04	1.59	0.873
		σ*(C18-H21)	0.00432	160.25	1.88	0.695
		σ*(C33-H35)	0.00338	65.09	2.08	0.466
		π*(C12-O17)	0.11130	54.43	0.05	0.071
σ(C12-C13)	0.98724	σ*(C5-C8)	0.00605	46.71	0.87	0.291
		(σ*C9-C11)	0.00707	6539.64	0.03	0.533
		σ*(C11-H16)	0.00715	83.40	0.71	0.307
		π*(C12-O17)	0.11130	40.43	0.62	0.211
		σ*(C13-C18)	0.00823	129.10	0.58	0.345
		σ*(C18-H21)	0.00432	60.87	0.87	0.291
σ(C13-C18)	0.98956	σ*(C5-C8)	0.00605	35.28	0.75	0.206
		σ*(C11-H16)	0.00715	84.84	0.59	0.284
		π*(C12-O17)	0.11130	31.66	0.51	0.169
		σ*(C13-C18)	0.00823	120.49	0.46	0.298
		σ*(C18-H21)	0.00432	56.14	0.75	0.261
σ(C33-H34)	0.99372	σ*(C5-C8)	0.00605	43.90	0.55	0.197
		σ*(C11-H16)	0.00715	121.57	0.39	0.275
		π*(C12-O17)	0.11130	51.77	0.31	0.168
		σ*(C13-C18)	0.00823	206.01	0.26	0.293
		σ*(C18-H21)	0.00432	62.52	0.55	0.197

σ(C33-H36)	0.99411	σ*(C3-C4)	0.01696	42.80	0.51	0.187
		σ*(C4-C6)	0.01556	41.48	0.57	0.196
		σ*(C5-C8)	0.00605	204.15	0.32	0.324
		σ*(C11-H16)	0.00715	724.23	0.16	0.433
		π*(C12-O17)	0.11130	501.77	0.08	0.264
		σ*(C13-C18)	0.00823	4158.41	0.03	0.461
		σ*(C18-H21)	0.00432	263.70	0.32	0.369
		σ*(C33-H35)	0.00338	68.61	0.53	0.240
n2 (O17)	0.95518	σ*(C11-H16)	0.00715	83.57	0.14	0.138
		π*(C12-O17)	0.11130	81.16	0.05	0.087
π*(C12-O17)	0.11130	σ*(C11-H16)	0.00715	119.28	0.08	0.367

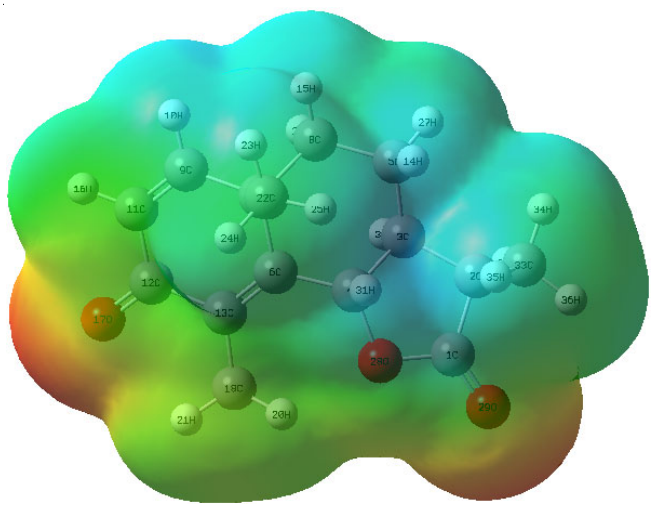

Fig. 5. MEP plot of α-santonin

investigation gives more donating tendency from electron givers to electron acceptors and the more prominent the degree of conjugation of the whole molecule [23]. As recorded in Table-2, the intramolecular interactions due to the orbitals of σ(C3-H30) with σ*(C9-C11), causing stabilization of 1455.58 kcal/mol and orbitals σ(C7-C8) with σ*(C9-C11), starting stabilization of 1579.14 kcal/mol. Moreover, the charge exchange from σ(C12-C13) to (σ*C9-C11) sums to the stabilization of 6539.64 kcal/mol and the charge exchange from σ(C33-H36) to σ*(C13-C18) degrees to the stabilization of 4158.41 kcal/mol. Also, the solid interaction (E(2) = 92.32 kcal/mol) was held between the σ(C1-O29) and σ* (C9-C11) orbital interaction. The stabilization energy of 81.16 kcal/mol is noticed between the lone pair (O17) orbital and π*(C12–O17) orbital, which is the characteristic highlight of pharmaceutical molecule α-santonin and these are all accounts for its bioactivity [24].

Thermodynamic parameters: The thermodynamic belongings of α-santonin by the DFT-B3LYP strategy are listed in Table-3. The optimized least energy for α-santonin is found to be -807.89494195 and -808.06886544 Hartrees, by lesser and higher basis sets. Higher the dipole moment, the more efficient will be the intermolecular interaction. In this work, the dipole moment and total energy of α-santonin are evaluated as 8.5071 Debye and 199.462 kcal mol^{-1}, respectively, by higher set calculations. The irrelevant zero-point vibrational energy is obtained (189.61475 kcal mol^{-1}) for α-santonin. The above thermodynamic limitations can be exploited in the assessment

TABLE-3
THERMODYNAMIC PROPERTIES OF α-SANTONIN

Parameters	Method/Basis set	
	B3LYP/6-31+G(d,p)	B3LYP/6-311++G(d,p)
Optimized global minimum energy (Hartrees)	-807.89494195	-808.06886544
Total energy (thermal), E_{total} (kcal mol^{-1})	201.373	199.462
Heat capacity, C_v (cal mol^{-1} k^{-1})	64.048	63.755
Entropy, S (cal mol^{-1} k^{-1})		
Total	126.007	122.514
Translational	42.403	42.403
Rotational	32.972	32.973
Vibrational	50.631	47.138
Vibrational energy, E_{vib} (kcal mol^{-1})	199.596	197.685
Zero point vibrational energy, (kcal mol^{-1})	191.23271	189.61475
Rotational constants (GHz)		
A	0.71374	0.71374
B	0.33054	0.33054
C	0.24818	0.24818
Dipole moment (Debye)	8.5658	8.5071

of chemical responses and to discover the extra thermodynamic energies of α-santonin.

Electronic properties: The UV-visible spectral study of α-santonin was measured by the highest occupied and lowest unoccupied molecular orbitals (HOMO-LUMO), which is the proficient degree of electron donor to acceptor region along the π-conjugated way. More profound information of frontier molecular orbital (FMOs) is composed primarily of π or π* orbitals [25]. The electronic properties of α-santonin from the theoretical calculations can portray the spectral highlights of the molecule, which are fulfilled by the time-dependent self-consistent field (TD-SCF) strategy. The computed energy transitions in 379.63 nm with energy = 3.2659 eV is noticed from HOMO to LUMO with 98% contribution by π→π* transition. The theoretical UV-vis range has appeared in Fig. 6. The energy of the orbitals computed at the B3LYP/6-311++G (d,p) level for the α-santonin is exposed in Fig. 7. In this study, α-santonin incorporates a profoundly functionalized ring with a cross coupled dienone framework and a lactone part. Subsequently, HOMO → LUMO transitions suggest an electron density exchange from the lactone bunch to the dienone framework. The energy gap between the normal and energized state was

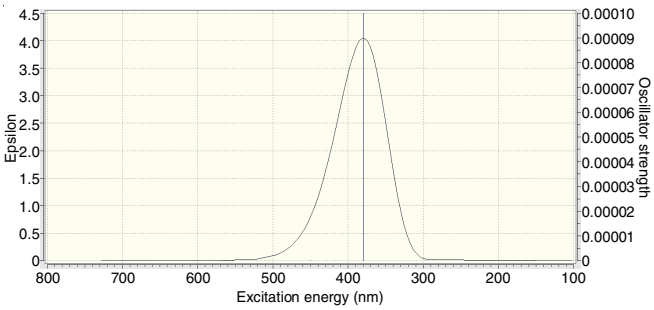

Fig. 6. UV plot of α-santonin

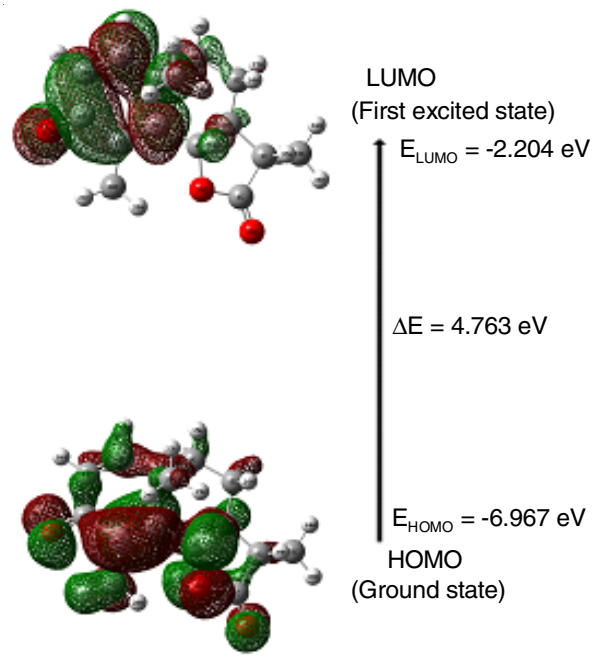

Fig. 7. HOMO-LUMO plot of α-santonin

found as 4.673 eV. Using Koopman's [25] hypothesis, the ionization potential (IP = - E_{HOMO} = -6.967 eV) was found from the energy difference between the radical cation and neutral molecule, whereas the electron affinity (EA = -E_{LUMO} = -2.204 eV) is computed from the energy difference between the neutral molecule and the anion. The other chemical properties are also reported in Table-4.

TABLE-4
HOMO-LUMO ENERGIES AND GLOBAL REACTIVITY DESCRIPTORS FOR α-SANTONIN

Molecular parameters	DFT-B3LYP/6-311++G(d,p)
HOMO (eV)	-6.967
LUMO (eV)	-2.204
ΔE (E_{HOMO} – E_{LUMO}) (eV)	4.763
Global hardness (eV)	2.3815
Global softness (eV^{-1})	0.2099
Electronegativity (eV)	4.5855
Global electrophilicity (eV)	4.414

Mulliken atomic charges: Mulliken charge scheming has a vital part in all the molecular systems, since atomic charges influence dipole moment and much additional things of molecular frameworks [26]. The overall charges of α-santonin received by Mulliken population investigation with the DFT-B3LYP strategy are recorded in Table-5. The negative charges on C3, C4, C5, C7, C8, C11, C12, O17, C18, C22, O28, O29 and C33 atoms in the aromatic ring drives the transformation of electron density. Due to these negative charge values, C6, C9, C13, H20 and H21 has positive charges and hence the molecule will be more acidic. Within the benzene ring, all hydrogen has a net positive charge. The graphical representation has been presented in Fig. 8.

TABLE-5
MULLIKEN CHARGES OF α-SANTONIN

Atoms	Atomic charges (Mulliken)		Atoms	Atomic charges (Mulliken)	
	B3LYP/6-31+G(d,p)	B3LYP/6-311++G(d,p)		B3LYP/6-31+G(d,p)	B3LYP/6-311++G(d,p)
C1	0.396	0.007	H19	0.222	0.291
C2	0.284	0.033	H20	0.253	0.378
C3	0.222	0.088	H21	0.226	0.269
C4	-1.166	-0.646	C22	-0.581	-1.211
C5	-0.599	-0.861	H23	0.213	0.269
C6	1.045	0.355	H24	0.234	0.292
C7	-0.905	-0.266	H25	0.204	0.202
C8	-0.225	-0.637	H26	0.228	0.314
C9	0.269	0.745	H27	0.213	0.289
H10	0.185	0.325	O28	-0.102	-0.053
C11	0.118	0.058	O29	-0.420	-0.312
C12	-0.086	-0.619	H30	0.235	0.394
C13	0.647	0.970	H31	0.237	0.430
H14	0.219	0.359	H32	0.237	0.373
H15	0.208	0.260	C33	-0.719	-0.964
H16	0.201	0.340	H34	0.213	0.237
O17	-0.472	-0.379	H35	0.208	0.276
C18	-1.109	-1.579	H36	0.232	0.279

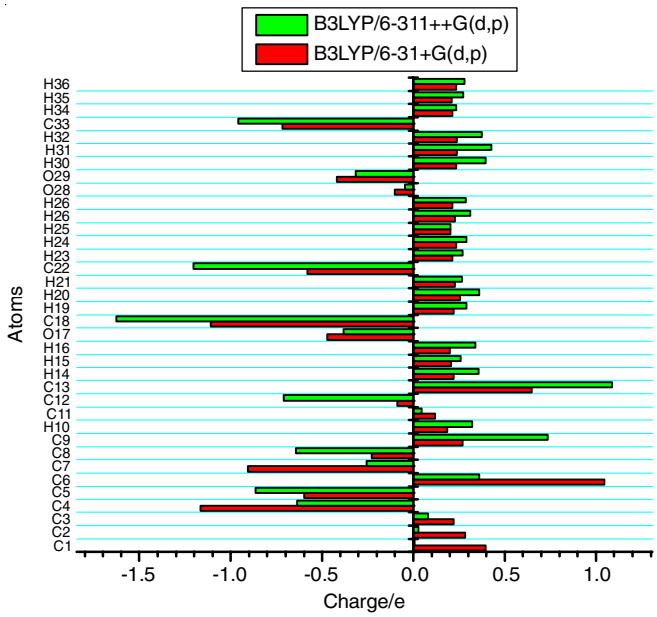

Fig. 8. Mulliken charges of α-santonin

NMR spectral analysis: The ^{13}C & ^{1}H NMR spectra of α-santonin have been analyzed by DFT/B3LYP with high basis set by implies of the Gauge-invariant atomic orbital (GIAO)

strategy. The computed ^{13}C and ^{1}H shift values of α-santonin with tetramethyl silane (TMS) as a reference are recorded in Table-6. Generally, the shifts were extended from 100 to 200 ppm for aromatic carbon systems [27]. In this study, the ^{13}C NMR chemical shifts of α-santonin are acquired within the range between 17.74 and 193.56 ppm. The oxygen atoms are deeply electronegative and diminishes the electron density at the C12 and C1 and consequently most extreme chemical shift is found at C12 and C1 (194.56 and 193.78 ppm). Further, the hydrogen atoms attached straight or adjacent electron acceptor atom, their shielding diminishes and the resonance leads to higher wavenumber. By contrast, hydrogens set closer to the electron donor atom rises the shielding effect, then resonance moved to lower wavenumber. In this condition, the computed shifts of H10 and H16 joined close to carbon atoms (C9 and C11) have the maximum value of 7.194 and 6.536 ppm, respectively. For the H atoms of methyl group, the shift values are < 3 ppm owing to the shielding impact.

TABLE-6
^{13}C NMR AND ^{1}H NMR CHEMICAL SHIFTS FOR α-SANTONIN

Atom	Chemical Shift DFT/6-311++G(d,p) (ppm)	Atom	Chemical Shift DFT/6-311++G(d,p) (ppm)
C12	194.56	H10	7.194
C1	193.78	H16	6.536
C9	162.45	H31	5.834
C6	161.38	H20	3.035
C13	136.61	H32	2.792
C11	128.86	H30	2.584
C4	92.09	H14	2.069
C3	59.63	H25	1.959
C7	54.72	H21	1.869
C2	49.76	H15	1.956
C8	45.92	H27	1.773
C22	31.96	H26	1.733
C5	29.11	H19	1.689
C18	18.33	H35	1.403
C33	17.74	H34	1.388
		H23	1.334
		H36	1.319
		H24	0.956

Conclusion

The molecular properties of α-santonin have been performed by using the DFT-B3LYP strategy with lower and higher basis sets. NBO outcomes explain that the charge exchange is primarily due to lone pair oxygens and π antibonding orbitals. The MEP outlines that the negative potentials are on oxygen atoms, together with the positive potentials (hydrogens), which give the reaction sites for α-santonin. To get the electronic interchanges and charge dispersion, the UV-visible spectra of the α-santonin have been calculated and the HOMO-LUMO energy separation was found to be 4.763 eV. The carbon and proton isotropic chemical shifts were calculated, which revealed the structural information of the molecule. Further, the docking studies showed that α-santonin may be a potential inhibitor against SARS-CoV-2 and cervical cancer infections.

CONFLICT OF INTEREST

The authors declare that there is no conflict of interests regarding the publication of this article.

REFERENCES

1. N. Kirtipal, S. Bharadwaj and S.G. Kang, *Infect. Genet. Evol.*, **85**, 104502 (2020); https://doi.org/10.1016/j.meegid.2020.104502
2. L.K. Penny and H.M. Wallace, *Chem. Soc. Rev.*, **44**, 8836 (2015); https://doi.org/10.1039/C5CS00705D
3. J. Ferlay, I. Soerjomataram, R. Dikshit, S. Eser, C. Mathers, M. Rebelo, D.M. Parkin, D. Forman and F. Bray, *Int. J. Cancer*, **136**, E359 (2015); https://doi.org/10.1002/ijc.29210
4. U. Mahantshetty, R. Engineer, H. Tongaonkar, J. Kulkarni, K. Dinshaw and S. Shrivastava, *J. Cancer Res. Ther.*, **9**, 672 (2013); https://doi.org/10.4103/0973-1482.126480
5. J.A. Green, J.M. Kirwan, J.F. Tierney, P. Symonds, L. Fresco, M. Collingwood and C.J. Williams, *Lancet*, **358**, 781 (2001); https://doi.org/10.1016/S0140-6736(01)05965-7
6. H. Lukka, H. Hirte, A. Fyles, G. Thomas, L. Elit, M. Johnston, M.F.K. Fung and G. Browman, *Clin. Oncol.*, **14**, 203 (2002); https://doi.org/10.1053/clon.2002.0076
7. J. Wang, S. Su, S. Zhang, S. Zhai, R. Sheng, W. Wu and R. Guo, *Eur. J. Med. Chem.*, **175**, 215 (2019); https://doi.org/10.1016/j.ejmech.2019.04.066
8. J. Khazir, P.P. Singh, D.M. Reddy, I. Hyder, S. Shafi, S.D. Sawant, G. Chashoo, A. Mahajan, M.S. Alam, A.K. Saxena, S. Arvinda, B.D. Gupta and H.M.S. Kumar, *Eur. J. Med. Chem.*, **63**, 279 (2013); https://doi.org/10.1016/j.ejmech.2013.01.003
9. F.F.P. Arantes, L.C.A. Barbosa, C.R.A. Maltha, A.J. Demuner, P. Marçal da Costa, J.R.O. Ferreira, L.V. Costa-Lotufo, M.O. Moraes and C. Pessoa, *Eur. J. Med. Chem.*, **45**, 6045 (2010); https://doi.org/10.1016/j.ejmech.2010.10.003
10. S. Palani, M. Jeyavijayan and K. Viswanathan, *Int. J. Recent Technol. Eng.*, **8**, 101 (2019); https://doi.org/10.35940/ijrte.D1039.1284S419
11. S.S.K. Goothy and A.H.S. Kumar, *BEMS Reports*, **6**, 1 (2020); https://doi.org/10.5530/bems.6.1.1
12. L. Bordoli, F. Kiefer, K. Arnold, P. Benkert, J. Battey and T. Schwede, *Nat. Protoc.*, **4**, 1 (2009); https://doi.org/10.1038/nprot.2008.197
13. Z. Yang, K. Lasker, D. Schneidman-Duhovny, B. Webb, C.C. Huang, E.F. Pettersen, T.D. Goddard, E.C. Meng, A. Sali and T.E. Ferrin, *J. Struct. Biol.*, **179**, 269 (2012); https://doi.org/10.1016/j.jsb.2011.09.006
14. O. Trott and A.J. Olson, *J. Comput. Chem.*, **31**, 455 (2010); https://doi.org/10.1002/jcc.21334
15. U. Viswanathan, S.M. Tomlinson, J.M. Fonner, S.A. Mock and S.J. Watowich, *J. Chem. Inf. Model.*, **54**, 2816 (2014); https://doi.org/10.1021/ci500531r
16. B.L. Narayana, D. Pran Kishore, C. Balakumar, K.V. Rao, R. Kaur, A.R. Rao, J.N. Murthy and M. Ravikumar, *Chem. Biol. Drug Des.*, **79**, 674 (2012); https://doi.org/10.1111/j.1747-0285.2011.01277.x
17. A.D. Becke, *J. Chem. Phys.*, **98**, 5648 (1993); https://doi.org/10.1063/1.464913
18. C. Lee, W. Yang and R.G. Parr, *Phys. Rev.*, **37**, 785 (1988); https://doi.org/10.1103/PhysRevB.37.785
19. M.J. Frisch, G.W. Trucks, H.B. Schlegal, G.E. Scuseria, M.A. Robb, J.R. Cheesman, V.G. Zakrzewski, J.A. Montgomerg Jr., R.E. Stratmann, J.C. Burant, S. Dapprich, J.M. Millam, A.D. Daniels, K.N. Kudin, M.C. Strain, O. Farkas, J. Tomasi, V. Barone, M. Cossi, B. Mennucci, R. Cammi, C. Pomelli, C. Adamo, S. Clifford, J. Ochterski, G.A. Petersson, P.Y. Ayala, Q. Cui, K. Morokuma, N. Rega, P. Salvador, J.J. Dannenberg, D.K. Malich, A.D. Rabuck, K. Raghavachari, J.B. Foresman, J. Cioslowski, J.V. Ortiz, A.G. Baboul, B.B. Stetanov, A. Liashenko, G. Liu, P. Piskorz, I. Komaromi, R. Gomperts, R.L. Martin, D.J. Fox, T. Keith, M.A. Al-Laham, C.Y. Peng, A. Nanayakkara, M. Challacombe,

P.M.W. Gill, B. Johnson, W. Chen, M.W. Wong, J.L. Andres, C. Gonzalez, M. Head-Gordon, E.S. Replogle and J.A. Pople, GAUSSIAN 09, Revision A 11.4, Gaussian, Inc, Pittsburgh PA (2009).
20. A. Sethi, K. Joshi, K. Sasikala and M. Alvala, *Intech Open*, (2019); https://doi.org/10.5772/intechopen.85991
21. F.J. Luque, J.M. Lopez and M. Orozco, *Theor. Chem. Acc.*, **103**, 343 (2000); https://doi.org/10.1007/s002149900013
22. S.D. Kanmazalp, M. Macit and N. Dege, *J. Mol. Struct.*, **1179**, 181 (2019); https://doi.org/10.1016/j.molstruc.2018.11.001
23. S. Jeyavijayan and P. Murugan, *Asian J. Chem.*, **33**, 83 (2020); https://doi.org/10.14233/ajchem.2021.22922
24. S. Premkumar, A. Jawahar, T. Mathavan, M.K. Dhas and A.M.F. Benial, *Spectrochim. Acta A Mol. Biomol. Spectrosc.*, **138**, 252 (2015); https://doi.org/10.1016/j.saa.2014.11.029
25. R. Mathammal, N. Sudha, L.G. Prasad, N. Ganga and V. Krishnakumar, *Spectrochim. Acta A Mol. Biomol. Spectrosc.*, **137**, 740 (2015); https://doi.org/10.1016/j.saa.2014.08.099
26. V.K. Rastogi, M.A. Palafox, R.P. Tanwar and L. Mittal, *Spectrochim. Acta A Mol. Biomol. Spectrosc.*, **58**, 1987 (2002); https://doi.org/10.1016/S1386-1425(01)00650-3
27. S. Jeyavijayan, *Spectrochim. Acta A Mol. Biomol. Spectrosc.*, **136**, 553 (2015); https://doi.org/10.1016/j.saa.2014.09.069